Engineering 7 (2021) 326–333

Contents lists available at ScienceDirect

Engineering

journal homepage: www.elsevier.com/locate/eng

Research
Green Chemical Engineering—Article

One-Step Preparation of Green Fabric for Continuous Antibacterial Applications

Rongkang Huang [a,b,#], Minghui Hu [a,b,#], Weiwen Liang [a,b,#], Juanjuan Zheng [c,#], Yang Du [d], Yanhuan Lin [d], Huaiming Wang [a,b], Wentai Guo [a,b], Zhantao Zeng [a,b], Chuangkun Li [a,b], Ming Li [e], Hui Wang [a,b,*], Xingcai Zhang [c,*]

[a] Department of Colorectal Surgery, The Sixth Affiliated Hospital of Sun Yat-sen University, Guangzhou 510655, China
[b] Guangdong Provincial Key Laboratory of Colorectal and Pelvic Floor Diseases, The Sixth Affiliated Hospital of Sun Yat-sen University, Guangzhou 510655, China
[c] John A. Paulson School of Engineering and Applied Sciences, Harvard University, Cambridge, MA 02138, USA
[d] Materials Science Institute, PCFM Lab and GDHPRC Lab, School of Chemistry, Sun Yat-sen University, Guangzhou 510275, China
[e] Department of Surgery, Dongguan Third Peoples' Hospital, Dongguan 523000, China

ARTICLE INFO

Article history:
Received 8 November 2019
Revised 20 June 2020
Accepted 6 August 2020
Available online 2 March 2021

Keywords:
Green chemistry
Polypropylene scaffold
Polydopamine
Triclosan
Antibacterial

ABSTRACT

Polypropylene (PP) scaffolds are the most commonly used biomedical scaffolds despite their disadvantages, which include problems with adhesion, infection, and inflammatory responses. Here, we report on the successful development of a facile one-step method to fabricate a series of novel triclosan polydopamine polypropylene (TPP) composite scaffolds and thereby effectively improve the biocompatibility and long-term antibacterial properties of PP scaffolds. The antibacterial triclosan can effectively interact with dopamine during biocompatible polydopamine formation on the PP scaffold by one-step green fabrication. Thanks to the sustained release of triclosan from the biocompatible polydopamine coating, a 5 mm × 5 mm sample of TPP-coated scaffold made with a triclosan concentration of 8 mg·mL^{-1} (referred to herein as TPP-8) exhibited a continuous antibacterial effect against both *Escherichia coli* (*E. coli*) and *Staphylococcus aureus* (*S. aureus*) for more than 15 d, at maximum antibacterial volumes of 2 and 5 mL, respectively. Our study establishes a new direction for facile long-term antibacterial studies for medical applications.

© 2021 THE AUTHORS. Published by Elsevier LTD on behalf of Chinese Academy of Engineering and Higher Education Press Limited Company. This is an open access article under the CC BY license (http://creativecommons.org/licenses/by/4.0/).

1. Introduction

With the development of modern medicine, an increasing number of polymeric materials, including polypropylene (PP), polylactic acid, polyurethane, polydopamine (PDA), and more, are being used in many medical fields [1–4]. Among these materials, medical PP materials have attracted considerable attention due to their light weight, diverse structure, and diverse physical and chemical properties, which are beneficial for many surgical applications [5–7].

Biological polymer scaffolds are a new medical material used to regenerate damaged and missing tissues *in situ*. Due to their high levels of compatibility, safety, and stability, as well as the fast recovery that ensues from their use, these scaffolds are attracting an increasing amount of attention from researchers [8,9]. For example, polylactic acid is a common biological scaffold material that has the disadvantage of decomposing into acidic substances in the human body, leading to local inflammatory reactions. Furthermore, it is difficult to match the degradation cycle of polylactic acid with the tissue growth cycle, which results in the loss of mechanical properties before the formation of new tissue, although this can be partly compensated for by the use of high-strength PP [10,11].

Traditional PP scaffolds are not very biocompatible and are therefore likely to cause a rejection of the immune system and local inflammation [12,13]. However, many studies have reported that PDA can be used to improve the biocompatibility of materials [14,15]. A successful coating of biocompatible PDA on top of a PP scaffold can greatly decrease the contact between PP and the body and thus greatly improve the biocompatibility of the scaffold.

* Corresponding authors.
E-mail addresses: wang89@mail.sysu.edu.cn (H. Wang), xingcai@mit.edu (X. Zhang).
# These authors contributed equally to this work.

https://doi.org/10.1016/j.eng.2020.08.022
2095-8099/© 2021 THE AUTHORS. Published by Elsevier LTD on behalf of Chinese Academy of Engineering and Higher Education Press Limited Company.
This is an open access article under the CC BY license (http://creativecommons.org/licenses/by/4.0/).

Triclosan is the most commonly used antibacterial drug [16–18], making it useful in the development of new antibacterial scaffolds.

Thus far, few studies have reported the use of a simple one-step method to achieve a functional coated scaffold. Herein, we develop a general and simple method for the preparation of an antibacterial biocompatible scaffold in which a mixture of PDA and triclosan is uniformly coated onto a medical PP scaffold. Experimental observations showed that the generated scaffold has a uniform loaded surface and good antibacterial properties. This approach can be further developed as a green universal preparation approach for antibacterial medicinal materials [19–22].

2. Materials and methods

2.1. Preparation of materials

In a typical synthesis, a piece of 2.5 cm × 2.5 cm PP scaffold (Jiangsu Sanlian Xinghai Medical Innovation Co. Ltd., China), 25 mL deionized water, 20 mL ethanol, 0.2 g F127 (a copolymer of epoxy propane and ethylene oxide), 0.2 g dopamine, and 0.2 g triclosan (highly hydrophobic) were placed in a flask with magnetic stirring for reaction under a weakly alkaline (pH 8.5) environment of tris–HCl solution. The reaction was stirred at room temperature (25 °C) for 24 h. Next, the as-obtained triclosan polydopamine polypropylene (TPP) scaffold was rinsed with deionized water and ethanol and then dried at 60 °C.

2.2. Characterizations

2.2.1. Material structure characterization

The morphology and composition of the samples were detected using field emission scanning electron microscopy (FESEM, JSM-6330F, JEOL Ltd., Japan). Fourier-transform infrared (FTIR) spectra were recorded using an Equinox 555 (Bruker, German) instrument from 400 to 4000 cm^{-1} with a 2 cm^{-1} resolution. X-ray photoelectron spectroscopy (XPS) measurements were performed on an ESCALab250 (Thermo Electron, USA) instrument, and the obtained results were calibrated by C 1s peak (284.8 eV) [23,24].

2.2.2. Antibacterial test

For the antibacterial test, *Escherichia coli* (*E. coli*, ATCC 25922) Gram-negative bacterial strains and *Staphylococcus aureus* (*S. aureus*, ATCC 6538) Gram-positive bacterial strains were precultured in sterilized Luria–Bertani broth (LB) overnight at 37 °C to obtain a concentration of approximately 10^7 colony-forming units (CFU) per milliliter.

2.2.3. Zone of inhibition

To determine the zone of inhibition [25], 200 μL of bacterial suspension was spread uniformly over the agar plates. TPP with a triclosan concentration of 4 mg·mL^{-1} (on a sample size of 5 mm × 5 mm) was put into every LB agar plate. The inoculated agars were incubated at 37 °C. The breadth of the inhibition zone was recorded after 24 h of incubation.

2.2.4. Minimum inhibitory concentration and minimum bactericidal concentration

To determine the minimum inhibitory concentration (MIC) and minimum bactericidal concentration (MBC) [26], a scaffold with a size of 5 mm × 5 mm was put into bacterial solution (5 mL) with different triclosan concentrations in the wells of a well plate, and then cultured at 180 r·min^{-1} for 24 h in a shaking bed at 37 °C. Next, 200 μL of the bacterial suspension was cultured on LB agar plates at 37 °C for 24 h. The colonies were counted after incubation for 24 h in order to investigate the bactericidal activity. The ager plates were examined for bactericidal growth; the last well that was clear indicated the MIC, while the plate containing the lowest triclosan concentration showing no growth indicated the MBC.

2.2.5. Continuous antibacterial test

For the continuous antibacterial test, different triclosan concentrations of TPP-coated scaffolds with a size of 5 mm × 5 mm was placed in a bacterial solution (5 mL) in different wells of a well plate, which was then cultured at 180 r·min^{-1} for 24 h in a shaking bed at 37 °C. The scaffold was taken out and rinsed three times with deionized water and then added to a new bacterial solution every 24 h of 15 d. After that, the optical density (OD) value of the former residual bacterial liquid was measured at every 24 h of 15 d. As triclosan is insoluble in water, washing could not reduce the triclosan content.

2.2.6. Triclosan sustained release test

For the triclosan sustained release test, a scaffold with a size of 5 mm × 5 mm was placed in phosphate-buffered saline (PBS) solution (5 mL) at 180 r·min^{-1} for 24 h in a shaking bed at 37 °C. The scaffold was removed and then added to new PBS solution every 24 h of 17 d, and the absorption value of the buffer solution at 281 nm was measured at 1, 3, 5, 7, 9, 11, 13, 15, and 17 d.

3. Results and discussion

3.1. Morphology and surface structure

Fig. 1 depicts the preparation procedure for the TPP-coated scaffold. The PP scaffold, dopamine, dispersant, and triclosan were mixed with water and ethanol in a beaker, and TPP was obtained by stirring the reaction mixture at room temperature for 24 h in a weakly alkaline environment adjusted by tris–HCl solution. Fig. 2 shows the scanning electron microscope (SEM) photos of the PP and TPP scaffolds and provides an element map of TPP. A comparison of Figs. 2(a) and (b) shows that the surface of the PP fiber bundle in the TPP-coated scaffold was coated by the triclosan PDA and had a rougher surface than the smooth PP fiber bundle surfaces reported in many published studies [27–29]. As shown in the Figs. 2(a) and (b), the morphology of the macro scaffold and the TPP scaffold changed from white to brown, indicating that the surface was coated with a mixture of PDA and triclosan. As shown in Figs. 2(d)–(g), the elements carbon (C), oxygen (O), nitrogen (N), and chlorine (Cl) were well distributed on the surface of the PP fiber. Energy dispersive X-ray (EDX) statistical results showed that the material contained 69.21% carbon, 21.33% oxygen, 1.88% nitrogen, and 7.58% chlorine. In this study, the triclosan content in the fabric was preliminarily determined by the element spectrum, as the element chlorine came from triclosan. We supplemented our analysis with element mapping and found that, as shown in Fig. 2(h), the content of Cl on the surface of the PP fibers increased as the triclosan concentration increased, indicating that the fabric was successfully modified by the triclosan.

Fig. 3 presents photographs and SEM images of the TPP mesh prepared with different triclosan concentrations of 1, 2, 4, and 8 mg·mL^{-1}, respectively. The photographs show that the color of the TPP obviously turned darker as the concentration of triclosan increased from 1 to 8 mg·mL^{-1}, although the SEM images did not show remarkable changes in morphology at a triclosan concentration of 2 mg·mL^{-1} or higher.

Based on the element mapping of Cl (Fig. 2(h)) on the surface of the TPP fiber at different concentrations, it was clear that the coating content improved as the concentration of triclosan increased from 1 to 4 mg·mL^{-1}. However, after the triclosan concentration reached 4 mg·mL^{-1}, the coating reaction was basically complete

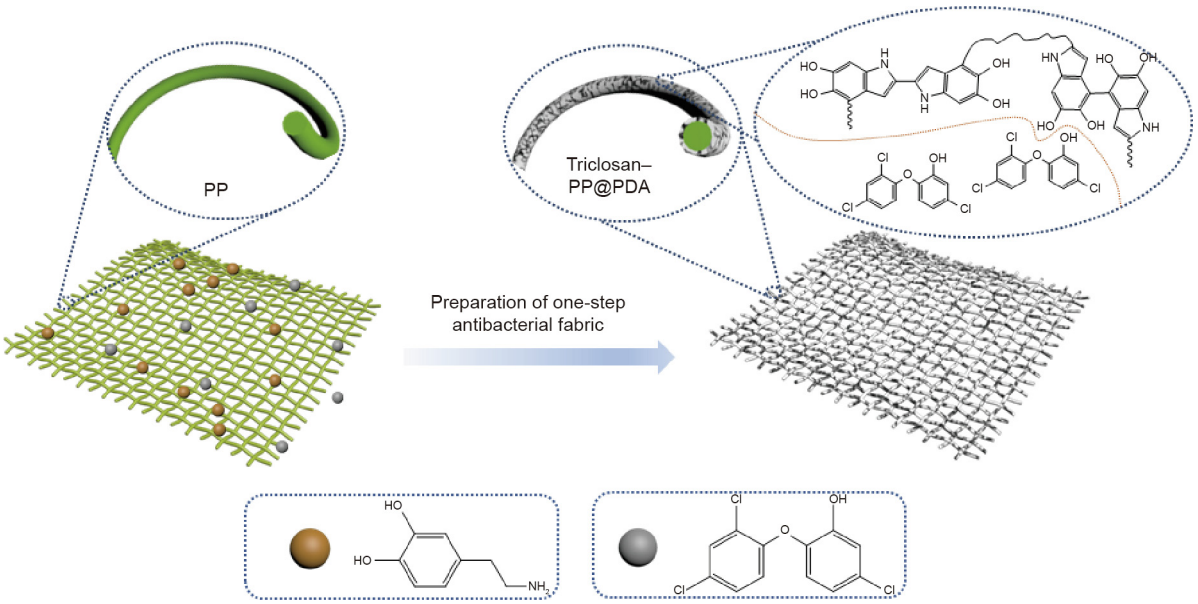

Fig. 1. Schematic diagram of the preparation of TPP fabric.

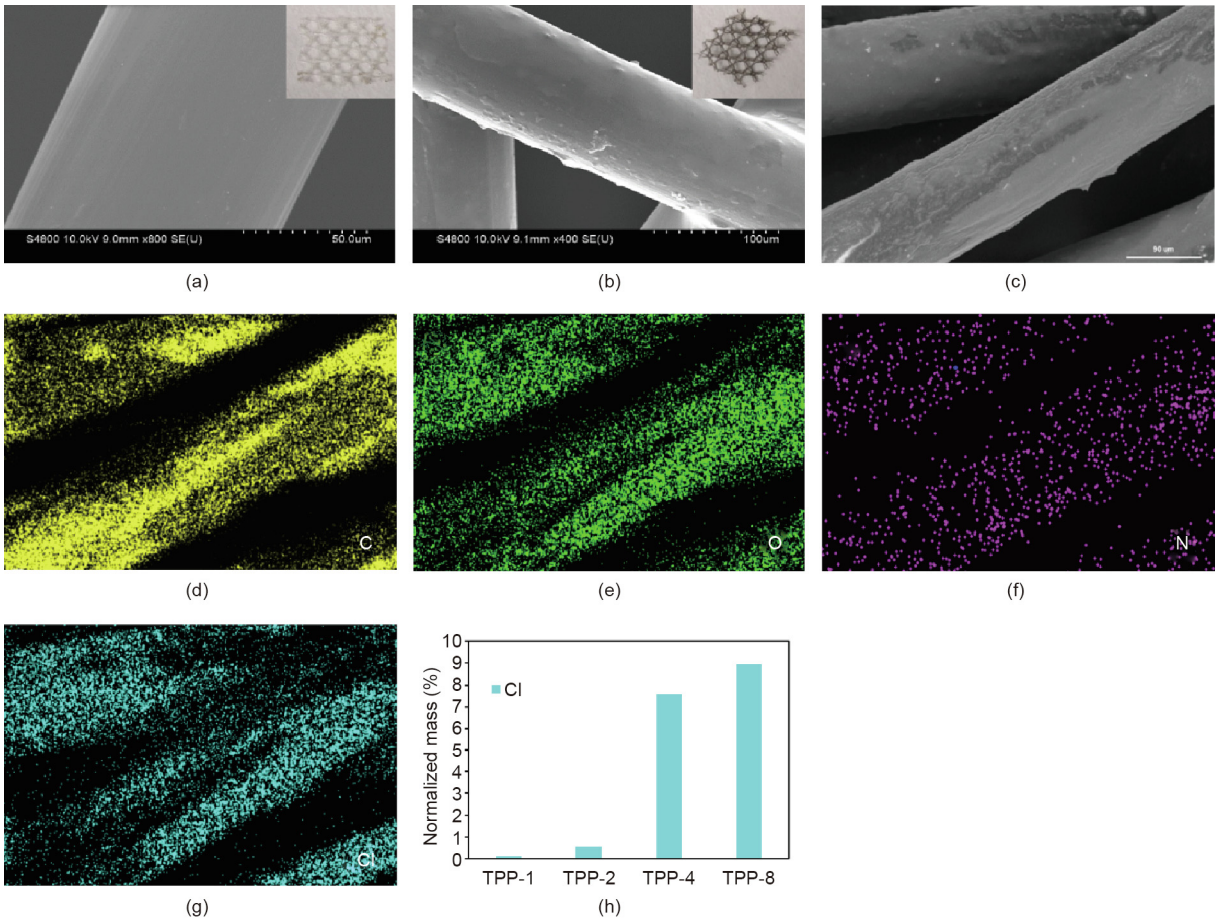

Fig. 2. (a, b) SEM images of the (a) PP and (b) TPP scaffold (inserts: photos of (a) PP and (b) TPP scaffold); (c) SEM image of the TPP scaffold which was used for element analysis; (d)–(g) images of the (d) C, (e) O, (f) N, and (g) Cl element distribution on a TPP scaffold with a triclosan concentration of 4 mg·mL^{-1}; (h) element mapping showing the Cl element in the TPP mesh for triclosan concentrations of 1, 2, 4, and 8 mg·mL^{-1}.

and did not show a marked improvement at higher concentrations. The subsequent antibacterial experiments revealed that the scaffold prepared with a triclosan concentration of 4 mg·mL^{-1} had the desired antibacterial and sterilization effect.

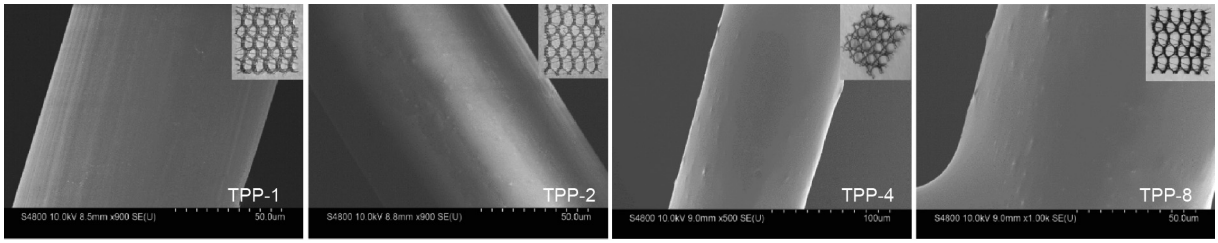

Fig. 3. Photographs and SEM images of TPP samples (a) TPP-1, (b) TPP-2, (c) TPP-4, and (d) TPP-8 with respective triclosan concentrations of 1 mg·mL^{-1}, 2 mg·mL^{-1}, 4 mg·mL^{-1}, and 8 mg·mL^{-1}, respectively.

Fig. 4 shows the infrared spectrum curves of PP, triclosan, PDA, and TPP. Because the PP scaffold was coated with PDA, the PP, PDA, and TPP curves show four absorption peaks within the range of 2955–2835 cm^{-1}, which are the symmetric and asymmetric vibration absorption peaks of methyl and methylene. For the PP curve, 1376 cm^{-1} is the characteristic peak of the methyl stretching vibration and 1460 cm^{-1} is the characteristic peak of the carbon–carbon stretching vibration (this peak appears in all samples) [30]. For the triclosan curve, 1110 cm^{-1} is the characteristic peak of the stretching vibration of the ether bond, 750–700 cm^{-1} is the characteristic peak of the stretching vibration of the carbon–chlorine bond in chlorobenzene, 1280 cm^{-1} is the deformation vibration peak of the hydroxy group, and 1203 cm^{-1} is the characteristic peak of the stretching vibration of the carbon–oxygen bond in phenol [31]. For the TPP curve, 1105 cm^{-1} is the characteristic peak of the carbon and nitrogen stretching vibration. The characteristic peaks of triclosan can also be observed, as described above.

The chemical composition of a material surface is an important piece of data in determining the properties of that material, and the morphology of triclosan and the distribution of chlorine are the determinants of antimicrobial activity. In order to further clarify the material surface structure, XPS results were obtained and calibrated by C 1s peak (284.8 eV). Fig. 5(a) shows the XPS spectrum. It can be clearly seen that the surface is rich in oxygen, nitrogen, chlorine, carbon, and other elements. Figs. 5(b)–(d) show the XPS spectra of high-resolution C 1s, O 1s, and Cl 2p, respectively. The high resolution of carbon in Fig. 5(b) is clearly composed of three peaks, which are electrons from C–C (284.3 eV), C–N (286.5 eV), and C–O (285.3 eV), respectively. The high resolution of oxygen in Fig. 5(c) is mainly composed of two peaks, H–O–C (534 eV) and C–O–C (532 eV), indicating that certain hydroxyl groups and ether groups in the triclosan exist on the surface of the material. Fig. 5(d) shows that the high-resolution Cl 2p spectrum is mainly composed of the two peaks of C–Cl (200.1 eV) and N–Cl (201.6 eV), indicating that the material has a high triclosan loading capacity. These findings also indicate that triclosan interacts with dopamine during synthesis, which is beneficial for triclosan loading.

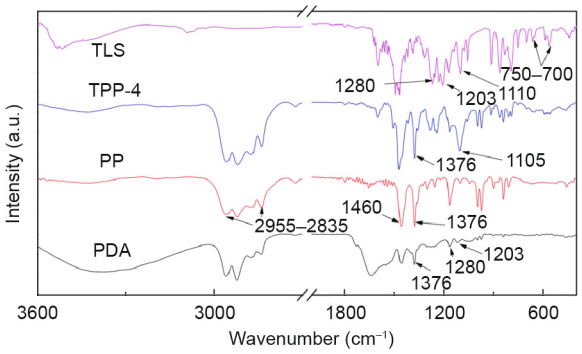

Fig. 4. Attenuated total reflection-infrared (TR-IR) spectra of triclosan (TLS), TPP-4 (the triclosan concentration is 4 mg·mL^{-1}), PP, and PDA.

3.2. Bactericidal and bacteriostatic properties

In order to evaluate the biological value of the materials, the bacteriostatic and bactericidal properties of the materials were evaluated using the bacteriostatic ring method. A total of 200 μL of bacterial suspension was spread uniformly over the agar plates. A 5 mm × 5 mm TPP scaffold was then placed in the center of the petri dish and incubated at 37 °C. The breadth of the inhibition zone was recorded after 24 h, as follows.

Figs. 6(a)–(c) show the bacteriostatic effect of cultivating 200 μL *S. aureus* for 24 h in the presence of TPP-1 (with a triclosan concentration of 1 mg·mL^{-1}), TPP-2 (with a triclosan concentration of 2 mg·mL^{-1}), and TPP-4 (with a triclosan concentration of 4 mg·mL^{-1}), respectively, for samples with a size of 5 mm × 5 mm. The TPP materials exhibited a good bacteriostatic effect against *S. aureus*, with the smallest bacteriostatic ring having a size of 2.6 cm (TPP-1) and the largest bacteriostatic ring having a size of 4.1 cm (TPP-4). Figs. 6(d)–(f) depict the bacteriostatic effect on *E. coli*, which was cultured for 24 h in the presence of TPP-1, TPP-2, and TPP-4, respectively, for samples with a size of 5 mm × 5 mm. The antibacterial effect of the material on *E. coli* was not as strong as that on *S. aureus*, but an obvious antibacterial effect was still exhibited, with a maximum antibacterial sanitation of 2.1 cm (TPP-4). This result of high antibacterial activity was consistent with the results from antibacterial commercial nonwoven fabrics designed by Karaszewska et al. [18], whose inhibition zone ranged from 3 to 6 mm after 12 months with antibacterial triclosan.

Fig. 7 shows the results of the experiment determining the MIC and MBC of TPP samples with different triclosan concentrations against *E. coli.* A TPP scaffold with a size of 5 mm × 5 mm was put into different volumes of bacterial liquid and incubated in a shaker at 37 °C for 24 h. Next, 200 μL was taken out and applied on agar medium and the culture was conducted at 37 °C for 24 h to observe the culture results. In Fig. 7, the bacterial liquid inside the red boxes was transparent, but strains appeared on the agar culture after 24 h. TPP-1 and TPP-2 exhibited a good antibacterial effect in 2 mL of bacterial liquid with a concentration of about 10^7 CFU·mL^{-1}, but had no obvious antibacterial effect in 5 mL of bacterial liquid with the same concentration. However, with the increase of triclosan concentration in TPP-4 and TPP-8 (with a triclosan concentration of 8 mg·mL^{-1}), these samples exhibited a good antibacterial effect in 5 mL of bacterial liquid with a concentration of about 10^7 CFU·mL^{-1}. In the 2 mL bacterial solution, no bacterial strains were found on TPP-4 and TPP-8 after being cultured for 24 h, indicating that TPP-4 and TPP-8 have a good bactericidal effect on 2 mL of bacterial liquid with a concentration of about 10^7 CFU·mL^{-1}.

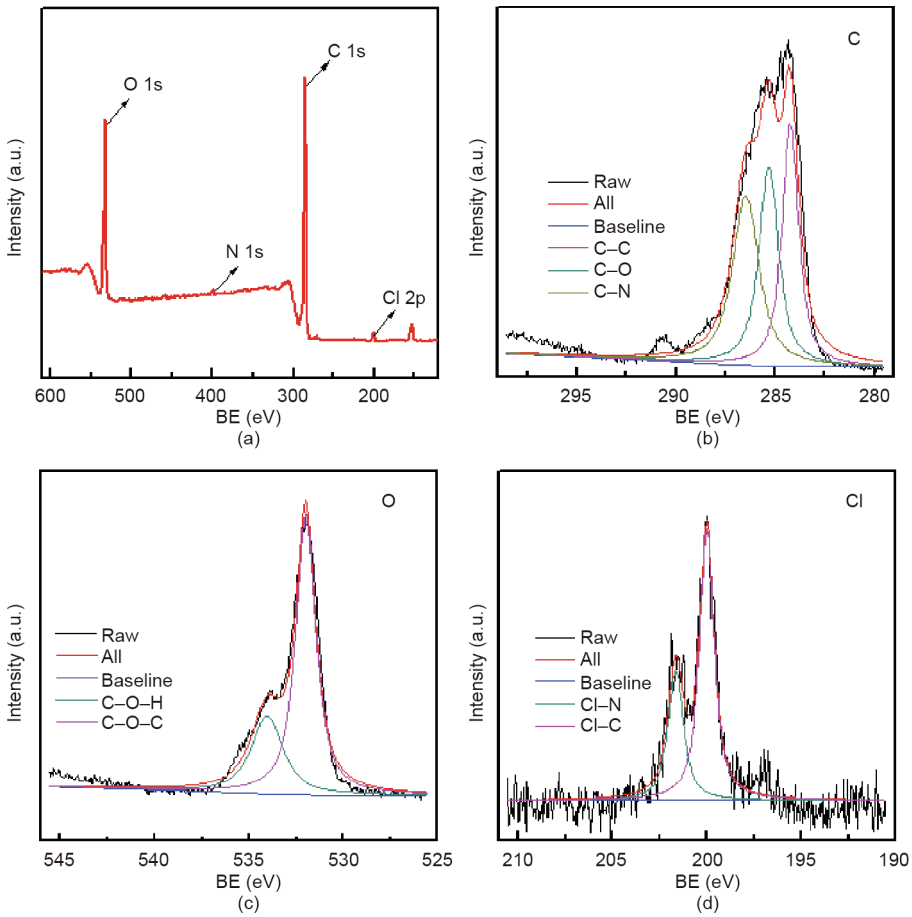

Fig. 5. XPS spectra of TPP with a triclosan concentration of 4 mg·mL^{-1}. (a) XPS spectrum; (b)–(d) XPS spectra of high-resolution (b) C 1s, (c) O 1s, and (d) Cl 2p. BE: binding energy.

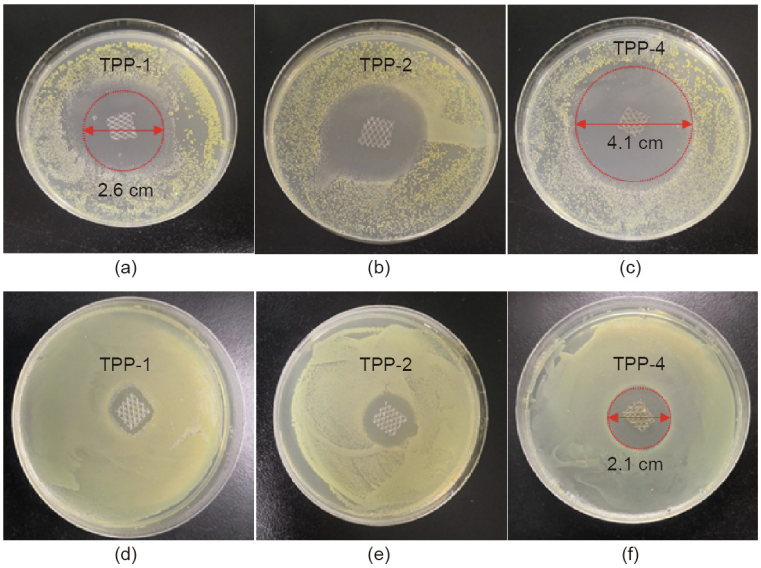

Fig. 6. Antibacterial performance against (a–c) *S. aureus* and (d–f) *E. coli.* with triclosan concentrations of 1, 2, and 4 mg·mL^{-1} for TPP-1, TPP-2, and TPP-4, respectively.

Fig. 8 shows the results from the experiment to determine the MIC and MBC of TPP samples with different triclosan concentrations against *S. aureus*. The bacterial liquids for the TPP-1 to TPP-4 samples were clear, as shown in the red box. After 200 μL of bacterial suspension was cultured on agar, obvious strains were found for TPP-1, TPP-2, and TPP-4, but no obvious strains were found for TPP-4 against 2 mL of *S. aureus* or for TPP-8 against 5 mL of *S. aureus*, as shown in the blue box. These findings indicate

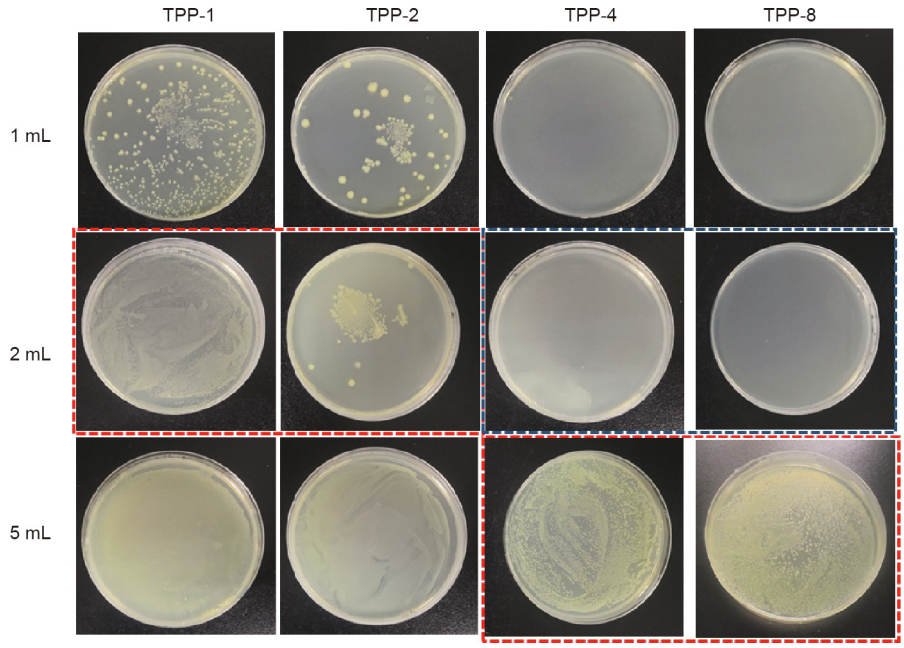

Fig. 7. MIC and MBC for TPP against *E. coli*. The labels "1 mL," "2 mL," and "5 mL" refer to 1, 2, and 5 mL of bacterial solution with a concentration of ~10^7 CFU·mL^{-1}. The triclosan concentrations are 1, 2, 4, and 8 mg·mL^{-1} for TPP-1, TPP-2, TPP-4, and TPP-8, respectively. Red box: The bacterial suspension was transparent, and the corresponding agar plates were examined and revealed bacterial growth. Blue box: The bacterial suspension was transparent, and the corresponding agar plates were examined and revealed no bacteria growth.

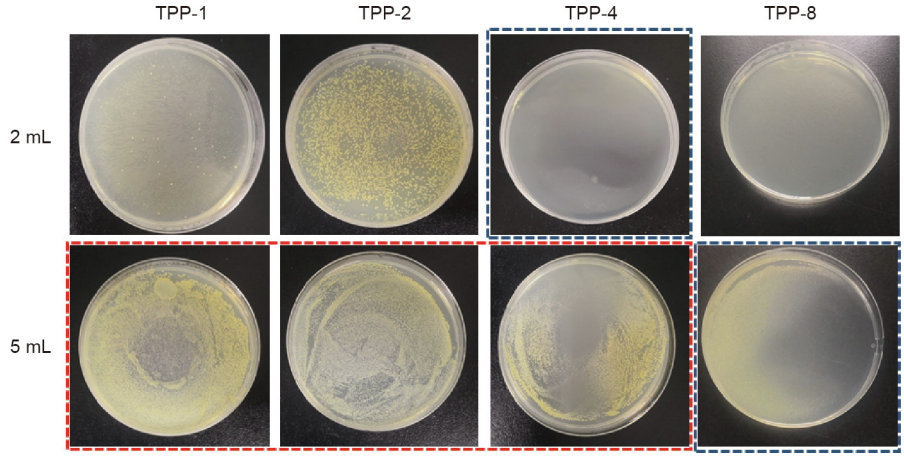

Fig. 8. MIC and MBC for TPP against *S. aureus*. The labels "2 mL" and "5 mL" indicate 2 and 5 mL, respectively, of bacterial solution with a concentration of ~10^7 CFU·mL^{-1}. The triclosan concentrations were 1, 2, 4, and 8 mg·mL^{-1} for TPP-1, TPP-2, TPP-4, and TPP-8, respectively. Red box: The bacteria suspension was transparent, and the corresponding agar plates were examined and revealed bacterial growth. Blue box: The bacterial suspension was transparent, and the corresponding agar plates were examined and revealed no bacteria growth.

that TPP-4 and TPP-8 have an obvious killing effect against 2 mL of *S. aureus* and 5 mL of *S. aureus*, respectively. It is clear that the prepared material has a good antibacterial and bactericidal effect, and has a better antibacterial effect toward *S. aureus* than toward *E. coli*.

3.3. Sustained antimicrobial activity and sustained release of triclosan by the TPP scaffold

In order to better illustrate the continuous antibacterial performance of the prepared materials, the prepared TPP scaffold (5 mm × 5 mm) and the comparison samples were cultured in a shaking bed for 24 h with 5 mL of bacteria liquid. The OD value of the bacteria was measured and recorded; the bacteria were then replaced with fresh bacteria. Fig. 9 shows the antibacterial persistence curves of the TPP scaffolds, PP, and F127. Fig. 9(a) shows the continuous antibacterial curve against *S. aureus*. The OD value of TPP-4 was still less than 0.2 on the 8th day under the test environment, indicating that the effective duration of TPP-4's continuous antibacterial time was 8 d. The effective duration of TPP-8's continuous antibacterial time was found to be more than 15 d. Based on a comparison with the PP and F127 comparison samples, it was clear that the antibacterial effect came from triclosan. As shown in Fig. 9(b), the effective antibacterial time against *E. coli* is 7 d for TPP-4 and more than 15 d for TPP-8.

In order to better understand the antibacterial mechanism, TPP-8 samples (5 mm × 5 mm) were placed in a PBS buffer solution and then placed in a shaker at 37 °C. The ultraviolet (UV) absorption spectrum of the solution was recorded on a daily basis and the buffer was changed every day. Fig. 10(a) shows the UV spectrum of TPP-8 and triclosan. The large characteristic peak of 230 nm is from

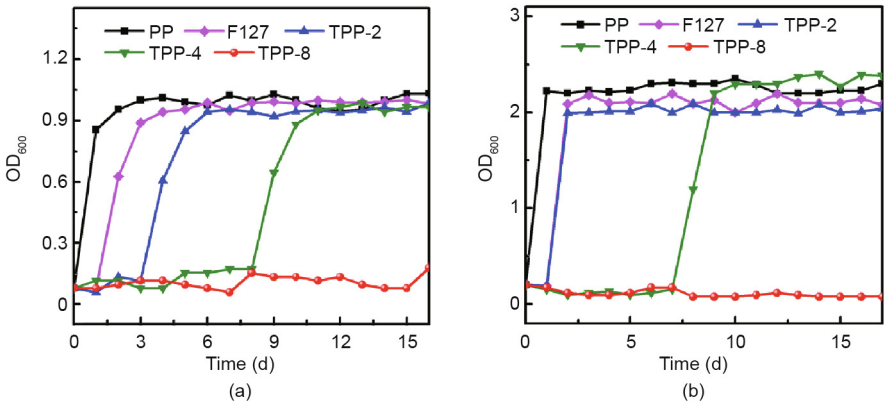

Fig. 9. The sustained antibacterial activity of a TPP patch against (a) *S. aureus* (5 mL) and (b) *E. coli* (5 mL). OD_{600}: OD value of a sample measured at a wavelength of 600 nm.

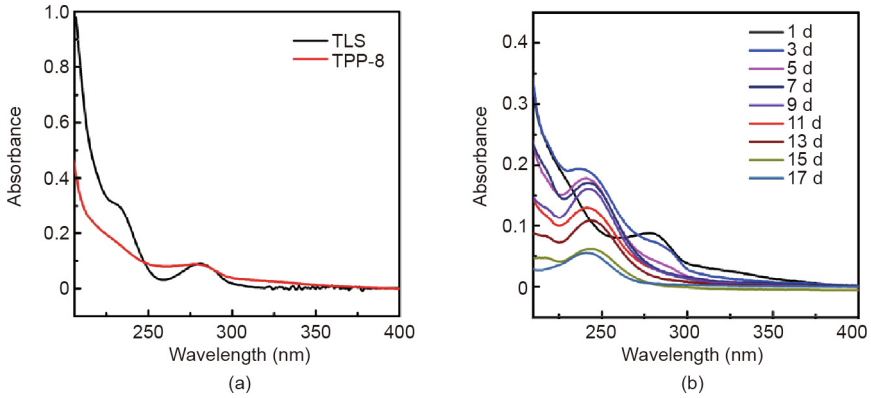

Fig. 10. Sustained-emission UV spectrum curve of TPP. (a) UV spectrum of TPP-8 and triclosan (TLS); (b) UV spectrum of TPP-8 at different times.

triclosan. Fig. 10(b) shows the UV spectrum of TPP-8 at different times. The characteristic absorption peak of triclosan decreases with the increment of time, but triclosan is still released at around 15 d, indicating that the sample has good sustained antibacterial performance.

4. Conclusion

In summary, we have demonstrated a simple yet efficient strategy for fabricating a medical PP scaffold coated with PDA that has been loaded with triclosan. The nanostructure and chemical composition of the TPP fiber was determined and the surface of the TPP fiber was found to be uniform and smooth, which indicates that triclosan PDA can form a good coating on PP fiber. Benefiting from the surface layer of PDA with triclosan, the functional PP products exhibited good antibacterial performances against *E. coli* and *S. aureus*. With an increase of triclosan concentration from 1 to 8 mg·mL^{-1}, the packing effect of the scaffold became more uniform and the antibacterial performance became stronger. The effective antimicrobial time is as long as 15 d in 5 mL of bacterial liquid with a concentration of about 10^7 CFU·mL^{-1}. The TPP composite effectively improved the biocompatibility and long-term antibacterial properties of a PP scaffold. Thus, TPP-coated scaffolds are promising candidates for future-generation ventral hernia repair materials, due to their ability to prevent bacteria contamination. Our findings facilitate the green fabrication of functional scaffold and fiber materials [32–36] for biomedical applications including wound dressing and catheters.

Acknowledgements

The authors gratefully acknowledge financial support from the project of the Science and Technology Program of Guangzhou (201704020059 and 201803010074).

Compliance with ethics guidelines

Rongkang Huang, Minghui Hu, Weiwen Liang, Juanjuan Zheng, Yang Du, Yanhuan Lin, Huaiming Wang, Wentai Guo, Zhantao Zeng, Chuangkun Li, Ming Li, Hui Wang, and Xingcai Zhang declare that they have no conflict of interest or financial conflicts to disclose.

References

[1] Parekh G, Shi Y, Zheng J, Zhang X, Leporatti S. Nano-carriers for targeted delivery and biomedical imaging enhancement. Ther Deliv 2018;9:451–68.
[2] Zhou M, Zhang X, Xie J, Qi R, Lu H, Leporatti S, et al. pH-sensitive poly(β-amino ester)s nanocarriers facilitate the inhibition of drug resistance in breast cancer cells. Nanomaterials 2018;8:952.
[3] Yang Y, Jin P, Zhang X, Ravichandran N, Ying H, Yu C, et al. New epigallocatechin gallate (EGCG) nanocomplexes co-assembled with 3-mercapto-1-hexanol and β-lactoglobulin for improvement of antitumor activity. J Biomed Nanotechnol 2017;13:805–14.
[4] Niu Y, Stadler FJ, He T, Zhang X, Yu Y, Chen S. Smart multifunctional polyurethane microcapsules for the quick release of anticancer drugs in BGC 823 and HeLa tumor cells. J Mater Chem B 2017;5:9477–81.
[5] Cazalini EM, Miyakawa W, Teodoro GR, Sobrinho ASS, Matieli JE, Massi M, et al. Antimicrobial and anti-biofilm properties of polypropylene meshes coated with metal-containing DLC thin films. J Mater Sci Mater Med 2017;28:97.
[6] Maitz MF. Applications of synthetic polymers in clinical medicine. Biosurface Biotribol 2015;1:161–76.

[7] Teo AJT, Mishra A, Park I, Kim YJ, Park WT, Yoon YJ. Polymeric biomaterials for medical implants and devices. ACS Biomater Sci Eng 2016;2:454–72.
[8] Hemamalini T, Giri Dev VR. Comprehensive review on electrospinning of starch polymer for biomedical applications. Int J Biol Macromol 2018;106:712–8.
[9] Saalwächter K, Seiffert S. Dynamics-based assessment of nanoscopic polymer-network mesh structures and their defects. Soft Matter 2018;14:1976–91.
[10] Kaito T, Myoui A, Takaoka K, Saito N, Nishikawa M, Tamai N, et al. Potentiation of the activity of bone morphogenetic protein-2 in bone regeneration by a PLA–PEG/hydroxyapatite composite. Biomaterials 2005;26(1):73–9.
[11] Lai Y, Li Y, Cao H, Long J, Wang X, Li L, et al. Osteogenic magnesium incorporated into PLGA/TCP porous scaffold by 3D printing for repairing challenging bone defect. Biomaterials 2019;197:207–19.
[12] Gonzalez R, Fugate K, McClusky D 3rd, Ritter EM, Lederman A, Dillehay D, et al. Relationship between tissue ingrowth and mesh contraction. World J Surg 2005;29:1038–43.
[13] Junge K, Klinge U, Rosch R, Klosterhalfen B, Schumpelick V. Functional and morphologic properties of a modified mesh for inguinal hernia repair. World J Surg 2002;26:1472–80.
[14] Hu M, Lin X, Huang R, Yang K, Liang Y, Zhang X, et al. Lightweight, highly permeable, biocompatible, and antiadhesive composite meshes for intraperitoneal repairs. Macromol Biosci 2018;18(7):1800067.
[15] Wang C, Wang D, Dai T, Xu P, Wu P, Zou Y, et al. Skin pigmentation-inspired polydopamine sunscreens. Adv Funct Mater 2018;28(33):1802127.
[16] Davachi SM, Kaffashi B, Torabinejad B, Zamanian A. *In-vitro* investigation and hydrolytic degradation of antibacterial nanocomposites based on PLLA/triclosan/nano-hydroxyapatite. Polymer 2016;83:101–10.
[17] Davachi SM, Kaffashi B, Torabinejad B, Zamanian A, Seyfi J, Hejazi I. Investigating thermal, mechanical and rheological properties of novel antibacterial hybrid nanocomposites based on PLLA/triclosan/nano-hydroxyapatite. Polymer 2016;90:232–41.
[18] Karaszewska A, Kamińska I, Kiwała M, Gadzinowski M, Gosecki M, Slomkowski S. Preparation and properties of textile materials modified with triclosan-loaded polylactide microparticles. Polym Adv Technol 2017;28(9):1185–93.
[19] Chen S, Zhang S, Galluzzi M, Li F, Zhang X, Yang X, et al. Insight into multifunctional polyester fabrics finished by one-step eco-friendly strategy. Chem Eng J 2019;358:634–42.
[20] Hou R, Wu L, Wang J, Yang Z, Tu Q, Zhang X, et al. Surface-degradable drug-eluting stent with anticoagulation, antiproliferation, and endothelialization functions. Biomolecules 2019;9:69.
[21] Jin L, Zhang X, Li Z, Chen G, Li J, Wang Z, et al. Three-dimensional nanofibrous microenvironment designed for the regulation of mesenchymal stem cells. Appl Nanosci 2018;8(8):1915–24.
[22] Li J, Li Z, Chu D, Jin L, Zhang X. Fabrication and biocompatibility of core–shell structured magnetic fibrous scaffold. J Biomed Nanotechnol 2019;15(3):500–6.
[23] Du Y, Khan S, Zhang X, Yu G, Liu R, Zheng B, et al. *In-situ* preparation of porous carbon nanosheets loaded with metal chalcogenides for a superior oxygen evolution reaction. Carbon 2019;149:144–51.
[24] Simons WW, editor. Sadtler handbook of infrared spectra. Philadelphia: Sadtler Research Laboratories; 1978.
[25] Wang X, Wang Y, Bi S, Wang Y, Chen X, Qiu L, et al. Optically transparent antibacterial films capable of healing multiple scratches. Adv Funct Mater 2014;24(3):403–11.
[26] McBride MC, Karl Malcolm R, David Woolfson A, Gorman SP. Persistence of antimicrobial activity through sustained release of triclosan from pegylated silicone elastomers. Biomaterials 2009;30(35):6739–47.
[27] Cao C, Tan L, Liu W, Ma J, Li L. Polydopamine coated electrospun poly(vinyldiene fluoride) nanofibrous membrane as separator for lithium-ion batteries. J Power Sources 2014;248:224–9.
[28] Cong Y, Xia T, Zou M, Li Z, Peng B, Guo D, et al. Mussel-inspired polydopamine coating as a versatile platform for synthesizing polystyrene/Ag nanocomposite particles with enhanced antibacterial activities. J Mater Chem B 2014;2(22):3450–61.
[29] Luo R, Tang L, Zhong S, Yang Z, Wang J, Weng Y, et al. *In vitro* investigation of enhanced hemocompatibility and endothelial cell proliferation associated with quinone-rich polydopamine coating. ACS Appl Mater Interfaces 2013;5(5):1704–14.
[30] Ortuso RD, Ricardi N, Bürgi T, Wesolowski TA, Sugihara K. The deconvolution analysis of ATR-FTIR spectra of diacetylene during UV exposure. Spectrochim Acta A 2019;219:23–32.
[31] Rodríguez-Félix DE, Castillo-Ortega MM, Nájera-Luna AL, Montaño-Figueroa AG, López-Peña IY, Del Castillo-Castro T, et al. Preparation and characterization of coaxial electrospun fibers containing triclosan for comparative study of release properties with amoxicillin and epicatechin. Curr Drug Deliv 2016;13(1):49–56.
[32] Li Z, Chu D, Chen G, Shi L, Jin L, Zhang X, et al. Biocompatible and biodegradable 3D double-network fibrous scaffold for excellent cell growth. J Biomed Nanotechnol 2019;15(11):2209–15.
[33] Wang X, Jin J, Hou R, Zhou Mi, Mou X, Xu K, et al. Differentiation of bMSCs on biocompatible, biodegradable, and biomimetic scaffolds for largely defected tissue repair. ACS Appl Biol Mater 2020;3(1):735–46.
[34] Huang R, Chen X, Dong Y, Zhang X, Wei Y, Yang Z, et al. MXene composite nanofibers for cell culture and tissue engineering. ACS Appl Biol Mater 2020;3(4):2125–31.
[35] Luo S, Wu S, Xu J, Zhang X, Zou L, Yao R, et al. Osteogenic differentiation of BMSCs on MoS_2 composite nanofibers with different cell seeding densities. Appl Nanosci 2020;10(9):3703–16.
[36] Bai Z, Wang L, Zhang X, Ran C, Liao Q, Qin L. A novel fiber-grafting-sensing testing method for temperature deformation of piezoelectric composites. Polym Test 2019;81:1061–2.